THE PUBLISHING HOUSE
OF THE ROMANIAN ACADEMY

PROCEEDINGS OF THE ROMANIAN ACADEMY, Series A,
Volume 23, Number 3/2022, pp. 247–257

OPTICAL AND MORPHOLOGICAL INVESTIGATIONS OF CHALCOGENIDE GE-SB-TE THIN FILMS

Nicoleta STAN, Nicoleta NEDELCU, Veturia CHIROIU, Ligia MUNTEANU, Marius IONESCU

Institute of Solid Mechanics, Romanian Academy, 15 Constatin Mille, 010141 Bucharest, Romania
Corresponding author: Nicoleta NEDELCU, E-mail: nicoleta_dulgheru@yahoo.com

Abstract. Chalcogenide thin films based on Ge-Sb-Te (GST) are synthesized from elements with 5N purity using the conventional melt-quenching method. The mixture was used as material for deposition on quartz substrate by the chemical vacuum deposition method. Optical and dielectric properties were determined by Spectro-ellipsometry measurements. The optical dispersion parameters are calculated using the single-oscillator model of Wemple-DiDomenico. The dissipation factor, the optical conductivity, the complex electric modulus, and the complex impedance of these GST layers were calculated. The AFM-SEM imagines revealed compact, continuous, and smooth films with good adhesion and uniform granules distribution.

Keywords: chalcogenide layer, thin film, dielectric properties, optical conductivity.

1. INTRODUCTION

Chalcogenide thin films based on Ge-Sb-Te (GST) are intensely studied due to optical, dielectric, and mechanical structural properties [1–3]. These materials are identified by a high enough contrast in electrical resistivity or optical phase-change memories parameters [4]. The changes from the amorphous state with high electrical resistivity to crystalline structure with low electrical resistivity are quantified by the Joule effect using an electric current pulse [5]. GST is an innovative material with high structural quality for phase change, offered by epitaxial films. Progress is made in the growth of crystalline phase change materials by physical methods, such as molecular beam epitaxy, sputtering, and pulsed laser deposition the difference and similarities between these physical deposition methods and the crystal structures of $Ge_2Sb_2Te_5$.

Over time a few methods were developed for chalcogenide layers, such as spin coating [6], magnetron sputtering [7, 8], thermal evaporation [9], atomic layer deposition [10], and metal-organic vapor phase epitaxy [11]. The Pulsed Laser Deposition (PLD) technique is suitable for the thin film growth of complex materials with good adhesion to the substrate and high homogeneity [12–18]. Experimentally technique discussed in above mentioned articles is important for the thin film growth because it show the reduction of cross-talk by greater than 30 times and the bending loss by greater than 3 times in densely integrated, ultra-compact photonic circuit blocks. By using a prototype, the dielectric metamaterial-waveguide property achieves a low propagation loss of approximately 3.7±1.0 dB/cm, comparable to those of silicon strip waveguides [12–14].

Growth of crystalline phase change materials by physical deposition methods is discussed in [19] and the phase-change materials for rewriteable data storage in [20]. Amorphous films such GeTe-Sb_2Te_3 and $GeSb_2Te_4$ or $Ge_2Sb_2Te_5$ present a large optical change and high-speed data rewriting which are important characteristics of optical memory material [21]. The growth depends on the electrical conductivity, surface morphology, crystallinity, and texture of the film. GST deposited on glasses substrate TiN and TiO_2 are higher-growth substrates, SiO2, Si_3N_4, and ZrO_2 are lower-growth substrate and HfO_2 is a non-growth substrate with no film growth [28, 29]. It is usually expected that the substrate dependency of the growth rate disappears after surface reconstruction is masked by a thicker film [22].

The optical and electrical properties of Ge-Sb-Te thin layers are compared between thermal evaporation (TE) and laser ablation. The ratio Sb/Te from the stoichiometric value in the TE samples [5] revealed a slight variation in chemical composition analysis.

The optical constants (refractive index and extinction coefficient) of thin films deposited by the PLD method presents higher values than those observed for the TE methods. High refractive index materials are commonly integrated with materials of contrasting refractivity to form transparent components with anti-reflective properties.

In this paper, the optical properties of the $Ge_xSb_{20-x}Te_{80}$ (GST) synthesized from elements with 5N purity (Ge, Sb, Te) are analyzed by using the Spectro-ellipsometry experimental data. The novelty of the paper consists in new observations on the optical properties and the photo-induced modifications in chalcogenide compositions.

Finally, the optical and morphological properties are discussed in connection with application of amorphous chalcogenides in plasmonic resonance structure configuration, binary chalcogenide photovoltaic cells and IR-coatings.

2. EXPERIMENTAL PROCEDURE

Three chalcogenide systems glassy $Ge_xSb_{20-x}Te_{80}$ (GST) alloys with composition x = 15, 17, and 19 at %, are synthesized from elements with 5N purity (Ge, Sb, Te) using the conventional melt-quenching method [23–32]. The mixture of the elements with proper weight percent was put in a quartz ampoule sealed down to 10^{-3} Pa pressure. The ampoules were heated to a rotary oven to 950°C, and to obtain homogeneous melting, the materials mixture was kept at this temperature for 24 hours by rotating the oven continuously. After finishing the process, the ampoules were removed, and the melts were cooled in ice water. The material mixture was used as material for deposition on quartz substrate by the thermal and chemical vacuum deposition method. Plasma cleaning discharge took place at 10^{-1} Pa, for 12 minutes in the atmosphere of N_2, and during this time, the dome is rotating (about 10 rot/min). This process is important because it removed the impurities on the walls from the vacuum deposition installation and activated the bulk before deposition. When the pressure has stabilized at 4×10^{-3} Pa, the heating resistance is coupled, ensuring a temperature of 300°C in the evaporation chamber while the dome is rotating with a 10rpm rotation speed. The material mixture was evaporated to 270 mA electric current. The optical monitoring control was done by TFCalc 3.5 software for approximately 3 min with a deposition rate of 6 nms^{-1} and showed 570 nm thickness. After evaporation, the samples were measured by the Spectro-Ellipsometry method using VASE Ellipsometer-Woollam. The surface quality of the films was characterized by scanning electron microscopy (SEM) and atomic force microscopy (AFM) using technology from ZEISS. The 2D AFM images for chalcogenide systems glassy $Ge_xSb_{20-x}Te_{80}$ alloys with composition x = 15, 17, and 19 at % were taken from a 5 μm×5μm scanned surface area.

3. RESULTS AND DISCUSSION

Ellipsometry measurements determined optical and dielectric properties. The experimental dates were recorded in the spectral range UV-VIS-NIR, in the spectral range 250–1350 nm, at 50^0 incidence angles. Fig. 1 shows the experimental dates ψ and Δ for chalcogenide systems glassy $Ge_xSb_{20-x}Te_{80}$ alloys with composition x = 15, 17, and 19 at %, with a mean square error (MSE) of less than 5 were obtained in the spectral range 250–1100 nm. The model presented in Fig. 2 contains two layers on the quartz substrate: roughness layer /chalcogen layer / substrate.

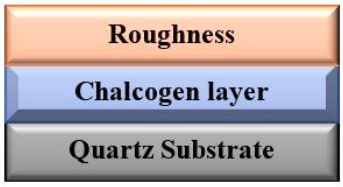

Fig. 2 – The model layers on the quartz substrate.

The Gauss and Lorentz oscillators simulated the chalcogenide layer by the General Oscillator method [33, 34]. The roughness layer, which is considered a mixture of 50% material (film) and 50% voids (air), was modeled with Bruggeman's effective medium approximation (B-EMA). The optical constants and thickness

are determined. The refractive index, n and extinction coefficient, *k*, according to photon energy, *hv* are presented in Fig. 3. The thickness for all alloys' chalcogenide composition is around 600 nm.

The absorption coefficient is calculated using the relation

$$\alpha(\lambda) = \frac{4\pi k}{\lambda}. \quad (1)$$

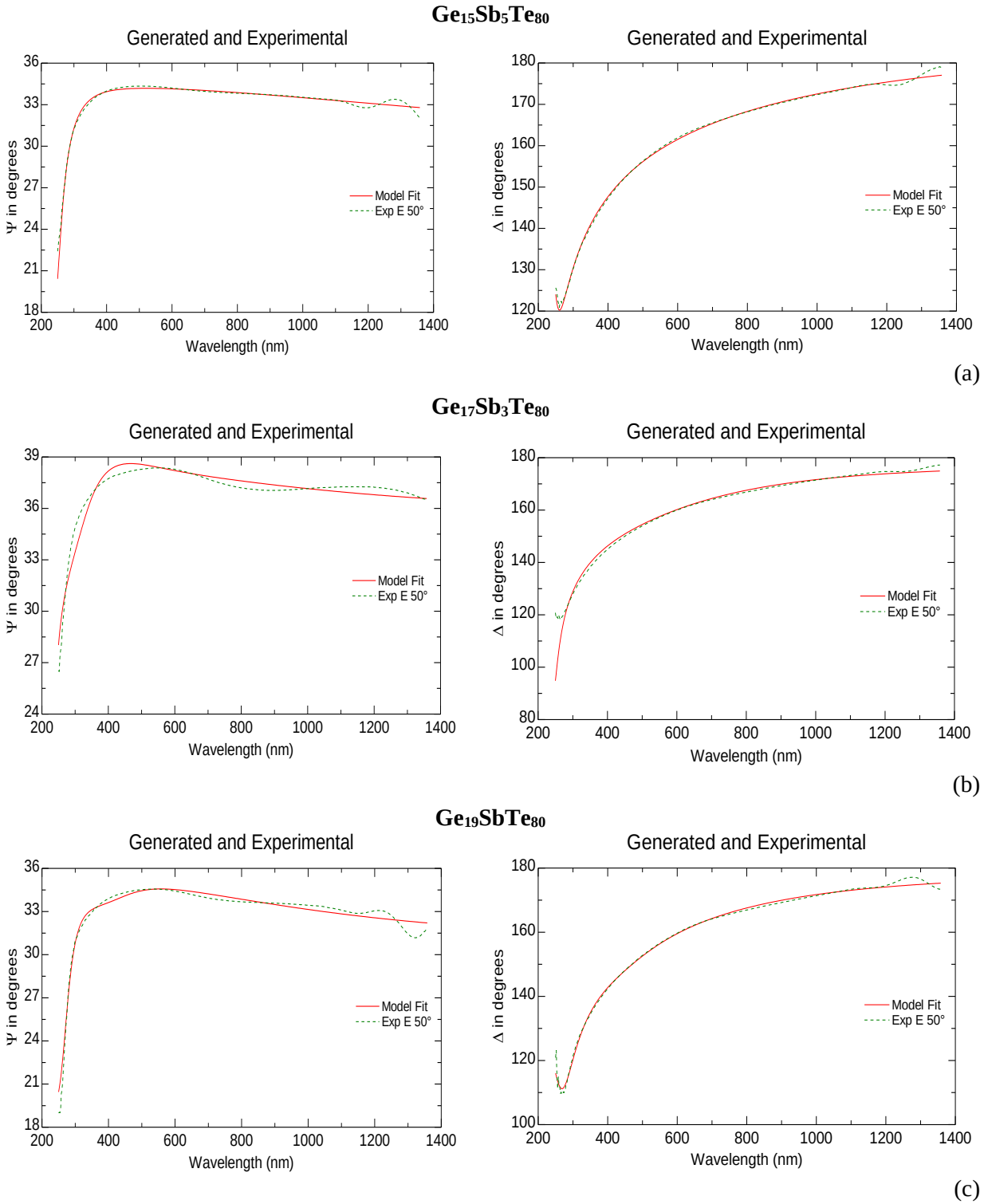

Fig. 1 – The experimental dates ψ and Δ for chalcogenide systems glassy $Ge_xSb_{20-x}e_{80}$ alloys with composition *x* = 15, 17, and 19 at %: a) ψ and Δ for $Ge_{15}Sb_5Te_{80}$; b) ψ and Δ for $Ge_{17}Sb3Te_{80}$; c) ψ and Δ for $Ge_{19}SbTe_{80}$.

Figure 4 shows the absorption coefficient versus photon energy, $h\nu$. According to Figs. 3 and 4, the constant optical decrease when germanium / antimony content increase / decrease. The relation between the absorption coefficient and the photon energy $h\upsilon$ is given by the relation developed by [35, 36]

$$\alpha = \frac{1}{h\nu}\left[\tilde{A}(h\nu) - E_g\right]^p, \tag{2}$$

where $\tilde{A}$ is constant depends on the transition probability, E_g is the width of the optical band gap, and p is an index that characterizes the optical absorption processes in the investigated films. The experimental analysis showed a proportionality between the absorption coefficient and the frequency of the photon energy in the form $(h\upsilon - E_g)^p$. The refractive index, the band gap and the oscillator parameters of amorphous GaSe thin films is discussed in [37] and the influence of temperature on charge transports and optical parameters for the $Ge_{15}Sb_5Se_{80}$ and $Ge_{15}Sb_5Te_{80}$ amorphous thin films in [38]. The behavior of the electronic dielectric constant in covalent and ionic materials is analyzed in [39]. The experimental results are based on the fundamental ε_2 spectrum, and it is found that for a certain choice of a model ε_2 spectrum, the bandgap parameter E_a in the high-frequency sum rule introduced by Hopfield, provides the connection between the single-oscillator parameters (E_0, E_d) and the static-dielectric-constant parameters (E_g, $\hbar\omega p$), i.e., $(\hbar\omega_p)^2 = E_a E_d$ and $E_g = (E_a E_0)^{1/2}$. Finally, it is suggested that the observed dependence of E_d on the coordination number and valency implies that an understanding of refractive-index behavior may lie in a localized molecular theory of optical transitions.

The exponent p defines the type of the optical transition in the chalcogenide films and should be one of these values: 2, 1/2, 3, and 3/2. Theoretically, p equals to 2, 1/2, 3, or 3/2 for the indirect allowed, direct allowed, indirectly forbidden, and directly forbidden transitions, respectively [40].

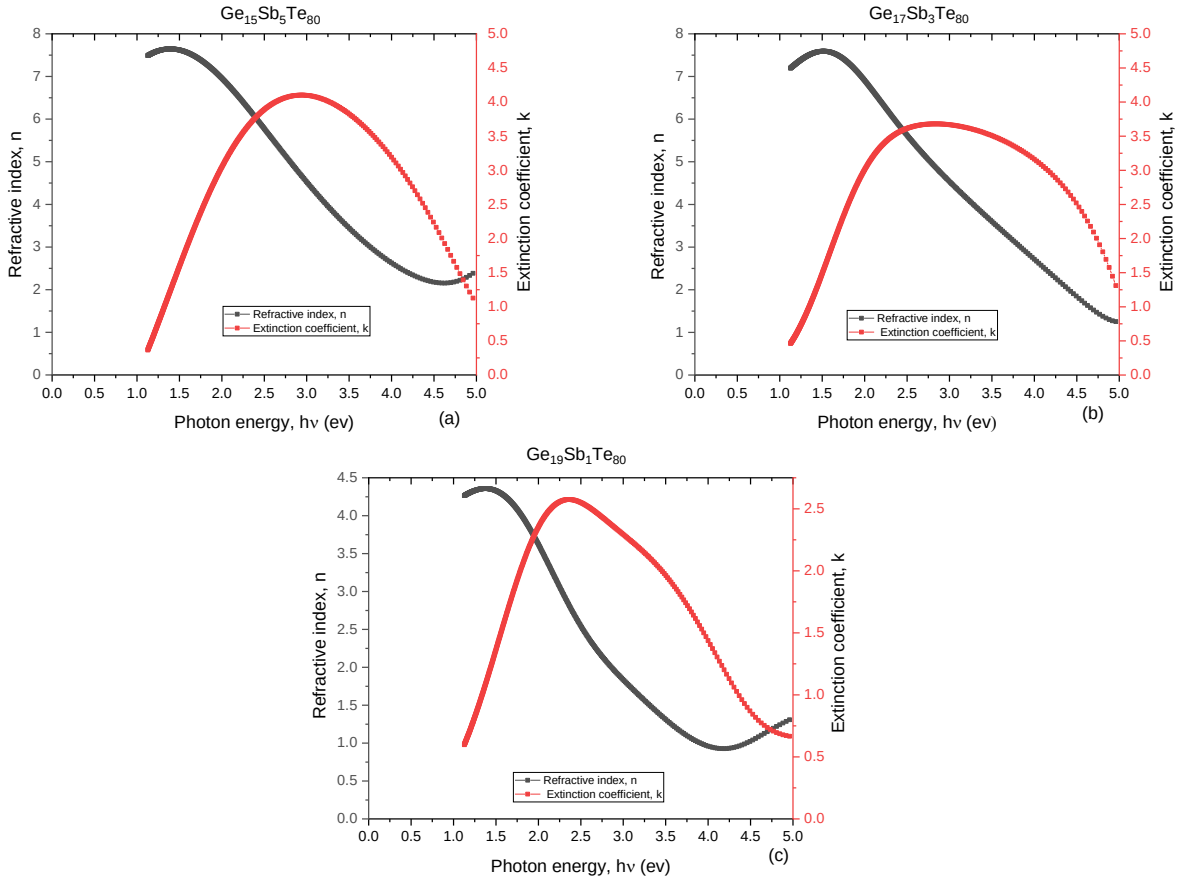

Fig. 3 – The optical constants, refractive index, n, and extinction coefficient, k, according to $h\nu$.

The usual method [31] for determining the optical transition includes plots of $(\alpha h\upsilon)^{1/p}$ versus the incident photon energy ($h\upsilon$). A set of plots is given by the exponent p: $(\alpha h\upsilon)^{1/2} - h\upsilon$; $(\alpha h\upsilon)^2 - h\upsilon$; $(\alpha h\upsilon)^{1/3} - h\upsilon$; and $(\alpha h\upsilon)^{2/3} - h\upsilon$. One of these plots determines the type of the optical transition and satisfies the widest linearity

of data in the high absorption region, the exponent p indicates that the dominant transition is a direct allowed one. Consequently, $(\alpha h\upsilon)^2$ was plotted against hυ in Fig. 5.

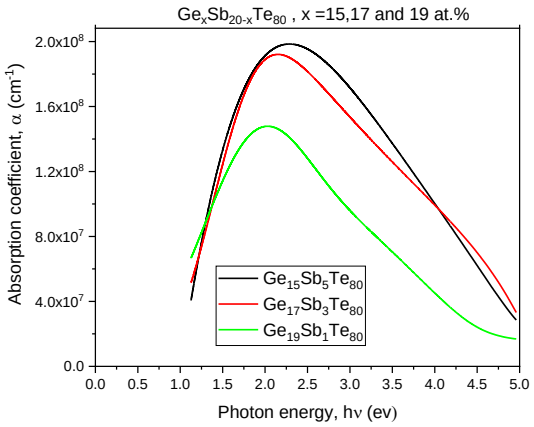

Fig. 4 – Absorption coefficient *versus* photon energy, *h*υ.

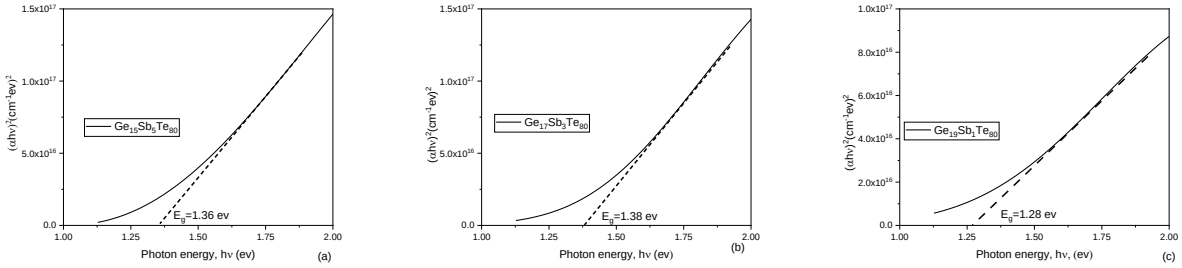

Fig. 5 – The plotted $(\alpha h\upsilon)^2$ *versus* photon energy *h*υ for: a) $Ge_{15}Sb_5Te_{80}$; b) $Ge_{17}Sb_3Te_{80}$; c) $Ge_{19}Sb_1Te_{80}$.

Influence of temperature on charge transports and optical parameters for the $Ge_{15}Sb_5Se_{80}$ and $Ge_{15}Sb_5Te_{80}$ amorphous thin films is studied in [32].

$Ge_xSb_{20-x}Te_{80}$ (GST) alloys with composition x = 15, 17, and 19 at %, were measured by VASE ellipsometer- Woollam. Using the UV-Vis-NIR spectra, the Urbach energy was detected in Fig. 6.

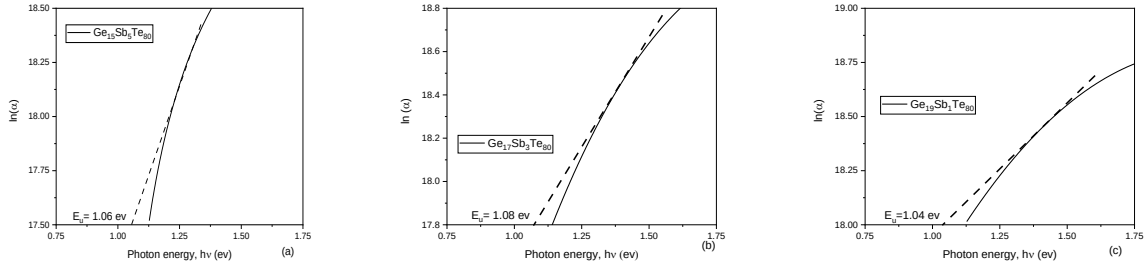

Fig. 6 – The variation of Urbach energy deduced by ln(α) of: a) $Ge_{15}Sb_5Te_{80}$; b) $Ge_{17}Sb_3Te_{80}$; c) $Ge_{19}Sb_1Te_{80}$.

The N_c value is the average coordination number of covalent bonds per atom and was calculated from the relation

$$N_c = [4(\chi)+3(40-\chi)+2(60)]/100\,, \tag{3}$$

where χ is the Ge content in at %, and the numbers 4, 3, and 2 are the valences of the elements Ge, Sb, and Te, respectively, the values of average coordination number N_c are present in Table 1. The variations on optical energy (band gap and Urbach energy) versus Germanium content are in Fig. 7. We can see the values of optical energy decrease when Germanium content increases.

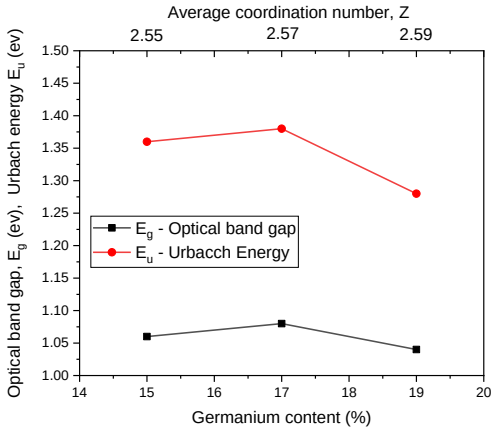

Fig. 7 – The variations on optical energy (Optical band gap E_g and Urbach energy E_u) versus Ge content (%).

Table 1

The average coordination number of covalent

Chalcogenide Layer	Coordination number (N_c)
$Ge_{15}Sb_5Te_{80}$	2.55
$Ge_{17}Sb_3Te_{80}$	2.57
$Ge_{19}Sb_1Te_{80}$	2.59

Dielectric function. The dielectric function is described by $\tilde{\varepsilon} = \varepsilon_1 + i\varepsilon_2$, where ε_1 is the real part that represents the normal dielectric constant, and ε_2 is the imaginary part that describes free-carrier absorption of the dielectric constant. The real part ε_1, and imaginary ε_2 [25] are described

$$\varepsilon_1 = n^2 - k^2 = \varepsilon_\infty - \left(\frac{e^2 N}{4\pi c^2 \varepsilon_0 m^*}\right)\lambda^2 = \varepsilon_\infty + 4\pi\chi_p, \tag{4}$$

$$\varepsilon_2 = 2nk = \left(\frac{\varepsilon_\infty \omega_p^{\ 2}}{8\pi^2 c^2 \tau}\right)\lambda^3, \tag{5}$$

where ω are the photon angular frequency, τ optical relaxation time, respectively, ε_∞ is the high-frequency dielectric constant, λ is the wavelength, the free charge carrier concentration, ε_0, is the permittivity of free space (8.854×10^{-12} F/m), m^* is the effective mass of the charge carrier, and c is the velocity of light, and χ_p is the electric susceptibility. The complex dielectric constant $\tilde{\varepsilon}$ completely describes the reflection, propagation, and light loss in the specimen structure, and therefore the material electronic structure can be clearly described. Fig. 8 represents the real, and the imaginary parts of the dielectric constants studied in photon energy ($h\upsilon$) range $Ge_xSb_{20-x}Te_{80}$ (GST) alloys with composition x = 15, 17, and 19 at %. We can see the values of the real and the imaginary parts of the dielectric constants decrease when Germanium content increase and Antimony content decrease.

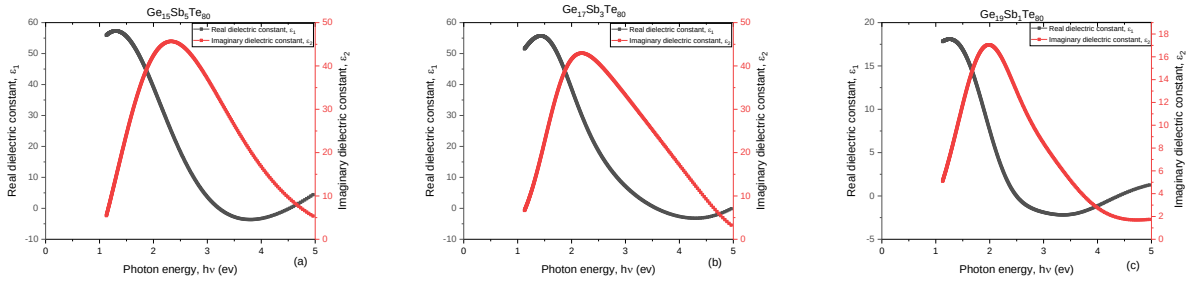

Fig. 8 – The real and the imaginary parts of the dielectric constants studied in photon energy ($h\upsilon$) range.

According to the oscillating simple model [33, 34], the real part of the permittivity is expressed by:

$$\varepsilon_1(\omega) = 1 + \omega_{p'}^2 \sum_i \frac{f_i}{\omega_i^{\ 2} - \omega^2}, \tag{6}$$

where $\omega_{p'}$ is the angular frequency of plasma, and f_i is the electric force of dipole oscillator for the transitions to the pulsation ω_i.

The expression of the permittivity becomes

$$\varepsilon_1(\omega)-1=n^2(h\nu)-1=\frac{E_d E_0}{{E_0}^2-(h\nu)^2}, \tag{7}$$

where E_d is the energy of dispersion which measures the average force of the optical transitions, E_0 is the energy of the simple oscillator. Using equations (4) and (7), we obtained the Wemple-DiDomenico model of refractive index's dispersion, which can be written as the representation $(n^2-1)^{-1}$ according to $(h\nu)^2$ on Fig. 9. After plotting the representation $(n^2-1)^{-1}$ according to $(h\nu)^2$ the linear part of the curves was extrapolated by the line $y=a-bx$ using the linear extrapolations of each curve deduce the values from the energy of the oscillator E_0 and dispersion E_d. The parameters a and b are related to the values of $E_0=\left(\sqrt{\frac{a}{b}}\right)$ and $E_d=\frac{1}{\sqrt{a\cdot b}}$.

The static dielectric constant permittivity (dielectric constant at zero frequency, ε_∞) is defined using equation (8).

$$\varepsilon_\infty=\varepsilon_1(0)=\lim_{\nu\to 0}\left[n^2(h\nu)\right]=1+\frac{E_d}{E_0}. \tag{8}$$

Table 2 indicates the values for E_0, E_d, n_0, and ε_∞ calculate for all chalcogenide systems. The values from dispersion energy increase while the other calculated parameters decrease when the germanium content increases.

The dissipation factor, tan δ, is described in equation (9) which is the power loss rate of the mechanical mode in a dissipative system [35].

$$\tan\delta=\frac{\varepsilon_2}{\varepsilon_1}. \tag{9}$$

Figure 10 plots the dissipation factor tan δ against $h\nu$ the for $Ge_xSb_{20-x}Te_{80}$ (GST) alloys with composition x = 15, 17, and 19 at %. As shown in Fig. 9, tan δ values display the same variation as the dielectric constants depicted in Fig. 8. The dissipation pick factor indicates interactions between the electrons; the interactions are also the origin of the peaks in the dielectric constant spectra.

Table 2

The values for E_0, E_d, n_0, ε_∞ calculate for $Ge_xSb_{20-x}e_{80}$ (GST) with composition x = 15, 17, and 19 at %

Thin film	**E_0 (ev)**	**E_d (ev)**	**n_0**	**ε_∞**
$Ge_{15}Sb_5Te_{80}$	1.59	13.66	3.09	9.55
$Ge_{17}Sb_3Te_{80}$	1.61	13.55	3.06	9.36
$Ge_{19}Sb_1Te_{80}$	1.91	13.15	2.81	7.89

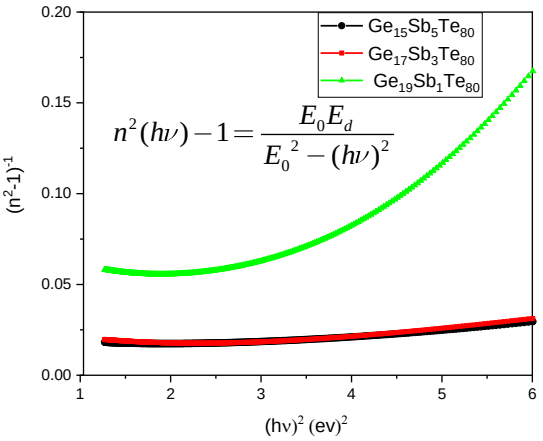

Fig. 9 – Wemple-DiDomenico plot.

We add here that the structural, optical spectroscopy, optical conductivity and dielectric properties of $BaTi_{0.5}(Fe_{0.33}W_{0.17})O_3$ and the electronic processes in noncrystalline materials are studied in [36, 37].

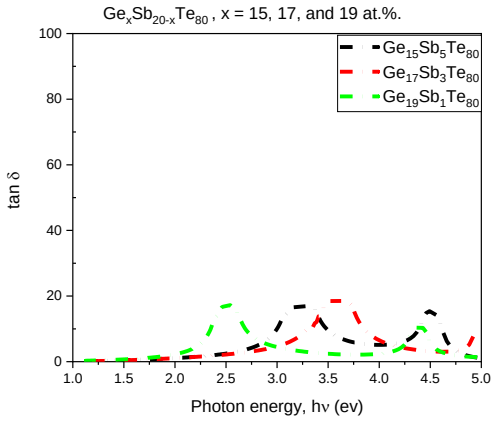

Fig. 10 – Spectral dependence of (tan δ) for $Ge_xSb_{20-x}Te_{80}$ with composition x = 15, 17, and 19 at %.

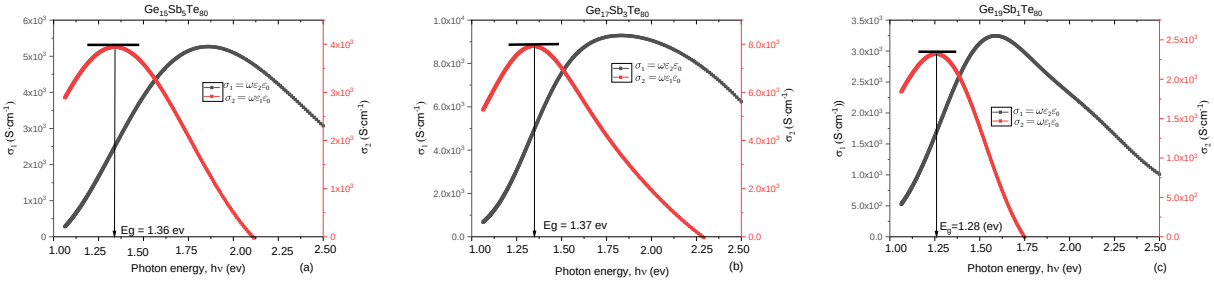

Fig. 11 – Spectral dependence of the real and imaginary parts of optical conductivity for $Ge_xSb_{20-x}Te_{80}$ (GST) alloys with composition x = 15, 17, and 19 at %: a) $Ge_{15}Sb_5Te_80$; b) $Ge_{17}Sb_3Te_{80}$; c) $Ge_{19}Sb_1Te_{80}$.

Having the values of ε_1 and ε_2 we obtained the complex electric modulus (Fig. 12) and the complex impedance (Fig. 13), by follows

$$Me^* = \frac{1}{\tilde{\varepsilon}} = Me_1 + iMe_2 = \frac{\varepsilon_1}{(\varepsilon_1^2 + \varepsilon_2^2)} + i\frac{\varepsilon_2}{(\varepsilon_1^2 + \varepsilon_2^2)}, \tag{10}$$

$$Z^* = \frac{1}{i\omega C_0 \tilde{\varepsilon}} = \frac{Me^*}{i\omega C_0} = Z_1 + iZ_2, \quad i^2 = -1, \tag{11}$$

where Me_1 and Me_2 are the real and imaginary parts of the electric modulus, respectively, Z_1 and Z_2 are the real and imaginary parts of the complex impedance, respectively, and $C_0 = \left(\frac{A}{d}\right)\varepsilon_0$ is the vacuum capacitance of the cell, A and d is the area and the thickness of chalcogenide layers, ε_0 is the free space dielectric constant. The complex electric modulus is a decisive parameter to acquire information about the relaxation mechanism.

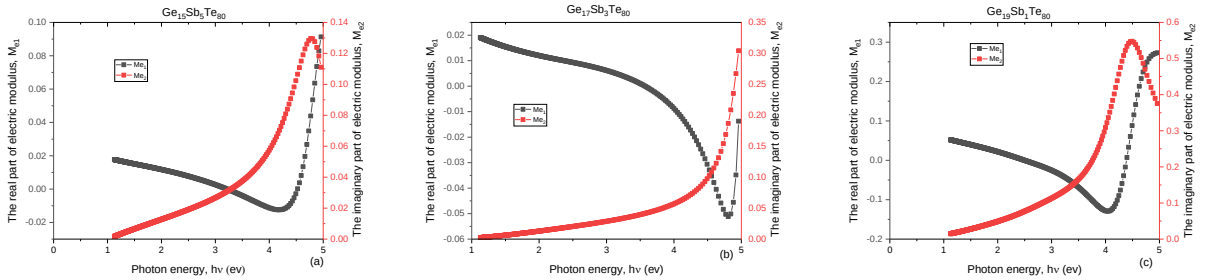

Fig. 12 – Variation of the complex electric modulus, Me^* for $Ge_xSb_{20-x}Te_{80}$ (GST) alloys with composition x = 15, 17, and 19 at %: a) $Ge_{15}Sb_5Te_80$; b) $Ge_{17}Sb_3Te_{80}$; c) $Ge_{19}Sb_1Te_{80}$.

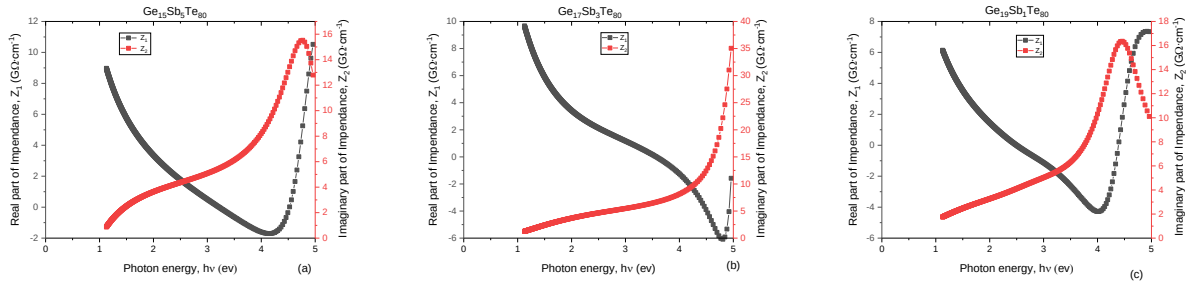

Fig. 13 – Variation of the complex impedance, Z^* for $Ge_xSb_{20-x}Te_{80}$ (GST) alloys with composition x = 15, 17, and 19 at %: a) $Ge_{15}Sb_5Te_80$; b) $Ge_{17}Sb_3Te_{80}$; c) $Ge_{19}Sb_1Te_{80}$.

Figure 13 shows the variation of the real and imaginary parts of the impedance as a function of energy photon. The AFM-SEM technology from ZEISS is used to study the surface's morphology. They are revealed in Fig. 14 compact, continuous, and smooth films. The surfaces are without cracks and digs, without exfoliation area with good adhesion, and have a uniform distribution of granules originating from the film structure, influenced by the deposition conditions (material evaporation phase). The root means square (RMS) roughness of the sample surfaces measured by AFM was 1.86 nm ($Ge_{15}Sb_5Te_{80}$), 2.04 nm ($Ge_{17}Sb_3Te_{80}$;), and 1.75 nm ($Ge_{19}Sb_1Te_{80}$).

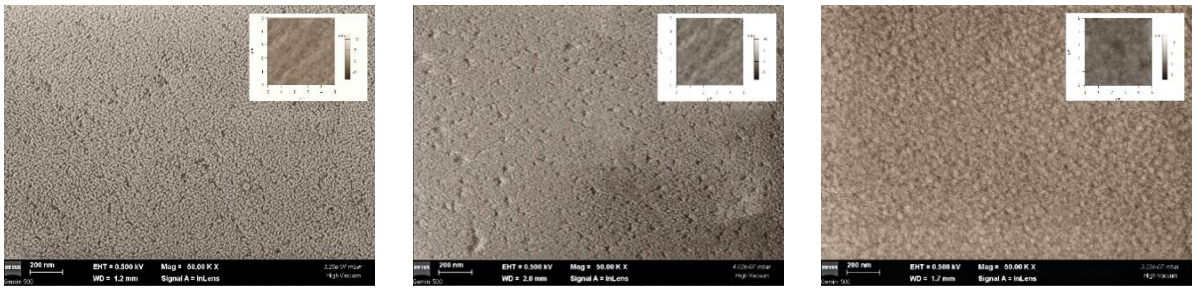

Fig. 14 – AFM and SEM images for $Ge_xSb_{20-x}Te_{80}$ (GST) alloys with composition x = 15, 17, and 19 at %: a) $Ge_{15}Sb_5Te_{80}$; b) $Ge_{17}Sb_3Te_{80}$; c) $Ge_{19}Sb_1Te_{80}$.

GST have applications in several branches of industry such as solar cells, electronic and optoelectronic devices at a low price.

This opens the door to control the structural and the optical properties of GST materials and leads to critical industrial applications such as solar cells, electronic and optoelectronic devices at a low price

4. CONCLUSIONS

The chalcogenide layers $Ge_xSb_{20-x}Te_{80}$ (GST) have been synthesized from elements with 5N purity (Ge, Sb, Te) using the conventional melt-quenching method. Structural and optical properties of GST layers are studied. The optical properties have been investigated by the Spectro-ellipsometry method. The refractive index and extinction coefficient decrease when germanium / antimony content increases/ decreases. Hight refractive index is obtained, and GST layers are commonly integrated like materials of contrasting refractivity to form transparent components with anti-reflective properties.

The optical absorption coefficient α, has shown a high value around the fundamental absorption edge and reflects the excellent quality of our samples demonstrate also by AFM and SEM imagines. The optical bandgap energy was estimated to be ~1.38 eV, which agrees with those reported by other authors. The optical dispersion parameters calculated by the single-oscillator model of Wemple-DiDomenico, show that the values from dispersion energy (E_d) increase while the others calculated parameters, the single-oscillator energy (E_0), the zero-frequency refractive index, and the dielectric constant at zero frequency, (ε_∞)decrease when the germanium content increases. The dissipation factor tan(δ), the optical conductivity (σ), the complex electric modulus (M^*), and the complex impedance (Z^*) of these GST layers were calculated. The AFM-SEM imagines

revealed compact, continuous, and smooth films with good adhesion and uniform granules originating from the film structure, influenced by the deposition conditions (material evaporation phase).

ACKNOWLEDGMENTS

This work was supported by a grant of the Romanian Ministry of Research and Innovation, project PN-IIIP2-2.1-PED-2019-0085 CONTRACT 447PED/2020 (Acronim POSEIDON).

REFERENCES

1. J.C. Phillips, *Topology of covalent non-crystalline solids I: Short-range order in chalcogenide alloys*, J. Non-Cryst. Solids, **34**, pp. 153–181,1979.
2. Pengfei GUO, Andrew M. SARANGAN, Imad AGHA, *A review of Germanium-Antimony-Telluride phase change materials for non-volatile memories and optical modulators*, Appl. Sci., **9**, art. 530, 2019.
3. H. DIEKER, M. WUTTIG, *Influence of deposition parameters on the properties of sputtered $Ge_2Sb_2Te_5$ films*, Thin Solid Film, **478**, pp. 248–251, 2005.
4. M. VLČEK, S. SCHROETER, J. ČECH, T. WÁGNER, T. GLASER, *Selective etching of chalcogenides and its application for fabrication of diffractive optical elements*, J. Non-Cryst. Solids, **326–327**, pp. 515–518, 2003.
5. G. BULAI, O. POMPILIAN, S. GURLUI, P. NEMEC, V. NAZABAL, N. CIMPOESU, B. CHAZALLON, C. FOCSA, *Ge-Sb-Te chalcogenide thin films deposited by nanosecond, picosecond, and femtosecond laser ablation*, Nanomaterials, **9**, *5*, art. 676, 2019.
6. L. WANG, C. YANG, J. WEN, B. XIONG, *Amorphization optimization of $Ge_2Sb_2Te_5$ media for electrical probe memory applications*, Nanometer, **8**, art. 368, 2018.
7. J. GUTWIRTH, T. WAGNER, P. BEZDICKA, M. HRDLICKA, M. VLCEK, M. FRUMAR, *On angle resolved RF magnetron sputtering of GeSbTe thin films*, J. Non-Cryst. Solids, **355**, pp. 1935–1938, 2009.
8. I. HILMI, B. RAUSCHENBACH, J.W. GERLACH, E. THELANDER, P. SCHUMACHER, J.W. GERLACH, B. RAUSCHENBACH, *Epitaxial $Ge_2Sb_2Te_5$ films on Si (111) prepared by pulsed laser deposition*, Thin Solid Films, **619**, pp. 81–85, 2016.
9. D.T. YIMAM, H. ZHANG, J. MOMAND, B.J. KOOI, *Pulsed laser deposited stoichiometric GaSb films for optoelectronic and phase change memory applications*, Materials Science in Semiconductor Processing, **133**, art. 105965, 2021.
10. J. LEE, S. CHOI, C. LEE, Y. KANG, D. KIM, *GeSbTe deposition for the PRAM application*, Appl. Surf. Sci., **253**, pp. 3969–3976, 2007.
11. G. MUSSLER, A. RATAJCZAK, M. VON DER AHE, H. DU, D. GRÜTZMACHER, *Metal organic vapor phase epitaxy of Ge1Sb2Te4 thin films on Si (111) substrate*, Appl. Phys. A, **125**, pp. 1–7, 2019.
12. S. JAHANI, S. KIM, J. ATKINSON, J.C. WIRTH, F. KALHOR, A.A. NOMAN, W.D. NEWMAN, *Controlling evanescent waves using silicon photonic all-dielectric metamaterials for dense integration*, Nature Communications, **9**, *1*, pp. 1893, 2018.
13. R.G. DECORBY, N. PONNAMPALAM, M.M. PAI, H.T. NGUYEN, P.K. DWIVEDI, *High index contrast waveguides in chalcogenide glass and polymer*, IEEE Journal of selected topics in quantum electronics, **11**, *2*, pp. 539–546, 2005.
14. W.D. NEWMAN, C.L. CORTES, J. ATKINSON, S. PRAMANIK, R.G. DECORBY, Z. JACOB, *Ferrell-Berreman modes in plasmonic epsilon-near-zero media*, Acs Photonics, **2**, *1*, pp. 2–7, 2015.
15. Anni LEHMUSKERO, Markku KUITTINEN, Pasi VAHIMAA, *Refractive index and extinction coefficient dependence of thin Al and Ir films on deposition technique and thickness*, Optics Express, **15**, *17*, 10744–10752, 2007.
16. M. KUWATA-GONOKAMI, N. SAITO, Y. INO, M. KAURANEN, K. JEFIMOVS, T. VALLIUS, J. TURUNEN, Y. SVIRKO, *Giant optical activity in quasi-two-dimensional planar nanostructures*, Phys. Rev. Lett., **95**, art. 227401, 2005.
17. K. JEFIMOVS, T. VALLIUS, V. KETTUNEN, M. KUITTINEN, J. TURUNEN, P. VAHIMAA, M. KAIPIAINEN, S. NENONEN, *Inductive grid filters for rejection of infrared radiation*, J. Mod. Opt., **51**, pp. 1651–1661, 2004.
18. P. ZULIANI, E. PALUMBO, M. BORGHI, G. DALLA LIBERA, R. ANNUNZIATA, *Engineering of chalcogenide materials for embedded applications of Phase Change Memory*, Solid State Electron., **111**, pp. 27–31, 2015.
19. Jos E. BOSCHKER, Raffaella CALARCO, *Growth of crystalline phase change materials by physical deposition methods*, Advances in Physics: X, **2**, *3*, pp. 675–694, 2017.
20. M. WUTTIG, N. YAMADA, *Phase-change materials for rewriteable data storage*, Nat. Mater., **6**, pp. 824–832, 2007.
21. N. YAMADA, E. OHNO, K. NISHIUCHI, N. AKAHIRA, M. TAKAO, *Rapid-phase transitions of GeTe-Sb2Te3 pseudobinary amorphous thin films for an optical disk memory*, Journal of Applied Physics, **69**, pp. 2849–2856, 1991.
22. B.J. CHOI, S. CHOI, T. EOM, S.W. RYU, D.-Y. CHO, J. HEO, H.J. KIM, C.S. HWANG, Y.J. KIM, S.K. HONG, *Influence of substrates on the nucleation and growth behaviors of Ge2Sb2Te5 films by combined plasma-enhanced atomic layer and chemical vapor deposition*, Chemistry of Materials, **21**, *12*, pp. 2386–2396, 2009.
23. M. LESKELA, V. PORE, T. HATANPAA, M. HEIKKILÄ, M. RITALA, A. SCHROTT, S. RAOUX, S. ROSSNAGEL, *Atomic layer deposition of materials for phase-change memories*, ECS Transactions, **25**, *4*, art. 399, 2009.
24. E.M. KNEEDLER, B.T. JONKER, P.M. THIBADO, R.J. WAGNER, B.V. SHANABROOK, L.J. WHITMAN, *Influence of substrate surface reconstruction on the growth and magnetic properties of Fe on GaAs* (001), Physical Review B, **56**, *13*, art. 8163, 1997.

25. G. BAKAN, *Electrothermal characterization of phase-change films and device*s, Anadolu Univ. Sci. Technol. A Appl. Sci. Eng., **18**, pp. 1057–1065, 2017.
26. N. NEDELCU, V. CHIROIU, L. MUNTEANU, I. GIRIP, *On the optical non-linearity in the GeSbSe chalcogenide glasses*, Material Research Express, **7**, art. 066403, 2021.
27. N. NEDELCU, V. CHIROIU, L. MUNTEANU, *Optimum GeSbSe layer design with respect to transmission and thickness*, Opt. Eng., **60**, *3*, art. 035109, 2021.
28. N. NEDELCU, V. CHIROIU, L. MUNTEANU, C. RUGINĂ, *Uncertainties of transmittance and absorbance measurements of the chalcogenide thin films*, Applied Physics A: Materials Science & Processing, **127**, art. 147, 2021.
29. N. NEDELCU (DULGHERU), V. CHIROIU, C. RUGINĂ, L. MUNTEANU, R. IOAN, I. GIRIP, C. DRAGNE, *Dielectric properties of GeSbSe glasses prepared by the conventional melt-quenching method*, Results in Physics, **16**, art. 102856, 2020.
30. N. NEDELCU, V. CHIROIU, L. MUNTEANU, I. GIRIP, C. RUGINĂ, A. LŐRINCZI, E. MATEI, A. SOBETKII, *Design of highly transparent conductive optical coatings optimized for the oblique angle of light incidence*, Applied Physics A: Materials Science & Processing, **127**, art. 575, 2021.
31. N. NEDELCU, V. CHIROIU, L. MUNTEANU, I. GIRIP, *Characterization of GeSbSe thin films synthesized by the conventional melt-quenching method*, Spectroscopy – IR Spectroscopy for today's Spectroscopists, **35**, *S3*, pp. 22–33, 2020.
32. N. NEDELCU, N. STAN, V. CHIROIU, *Subharmonic generation in GeSbSe chalcogenide Cantor-like glasses*, Romanian Journal of Mechanics, **6**, *1*, pp. 3–14, 2021.
33. S. MISHRA, P. JAISWAL, D.K. DWIVEDI, *Chalcogenide glasses for sensor application: A review*, 5th IEEE Uttar Section International Conference on Electrical and Computer Engineering (UPCON), 2018.
34. J.-W. PARK, S.H. EOM, H. LEE, J.L.F. DA SILVA, Y.-S. KANG, T.-Y. LEE, Y.H. KHANG, *Optical properties of pseudobinary GeTe, $Ge_2Sb_2Te_5$, $GeSb_2Te_4$, $GeSb_4Te_7$, and Sb_2Te_3 from ellipsometry and density functional theory*, Phys. Rev. B, **80**, art. 115209, 2009.
35. J.I. PANKOVE, *Optical processes in semiconductors*, Prentice-Hall, New Jersey, 1971, p. 93.
36. J. TAUC, *Amorphous and liquid semiconductors*, Plenum, New York, 1974, Chap. 4.
37. A.F. QASRAWI, *Refractive index, band gap and oscillator parameters of amorphous GaSe thin films*, Cryst. Res. Technol., **40**, pp. 610–614, 2005.
38. A.M. BARD, F. ABDEL-WAHAAB, I.M. ASHRAF, *Influence of temperature on charge transports and optical parameters for the $Ge_{15}Sb_5Se_{80}$ and $Ge_{15}Sb_5Te_{80}$ amorphous thin films*, International Journal of Physical Sciences, **4**, *5*, pp. 313–320, 2009.
39. S.H. WEMPLE, M. DiDOMENICO, *Behavior of the electronic dielectric constant in covalent and Ionic Materials*, Phys. Rev. B, **3**, art. 1338, 1971.
40. Hossam DONYA, T.A. TAHA, *Preparation, structure and optical properties of ZnTe and PbTe nanocrystals grown in fluorophosphate glass*, Journal of Materials Science: Materials in Electronics, **29**, *10*, pp. 8610–8616, 2018.
41. M. FADEL, S.A. FAYEK, M.O. ABOU-HELAL, M.M. IBRAHIM, A.M. SHAKRA, *Structural and optical properties of SeGe and SeGeX (X = In, Sb and Bi) amorphous films*, J. Alloy. Compd., **485**, *1–2*, p. 604–609, 2009.
42. F. BOURGUIBA, A. DHAHRI, T. THARI, K. TAIBI, J. DHAHRI, E.K. HLIL, *Structural, optical spectroscopy, optical conductivity and dielectric properties of $BaTi_{0.5}(Fe_{0.33}W_{0.17})O_3$ perovskite ceramic*, Bull. Mater. Sci., **39**, *7*, pp. 1765–1774, 2016.
43. N.F. MOTT, E.A. DAVIS, *Electronic processes in noncrystalline materials*, Clarendon Press, Oxford, 1979.

Received January 27, 2022